Aerodynamic Design of the Hybrid Wing Body Propulsion-Airframe Integration

May-Fun Liou[1], Hyoungjin Kim[2], ByungJoon Lee[3], and Meng-Sing Liou[4]

NASA Glenn Research Center, Cleveland, Ohio, 44135

Abstract

A hybrid wingbody (HWB) concept is being considered by NASA as a potential subsonic transport aircraft that meets aerodynamic, fuel, emission, and noise goals in the time frame of the 2030s. While the concept promises advantages over conventional wing-and-tube aircraft, it poses unknowns and risks, thus requiring in-depth and broad assessments. Specifically, the configuration entails a tight integration of the airframe and propulsion geometries; the aerodynamic impact has to be carefully evaluated. With the propulsion nacelle installed on the (upper) body, the lift and drag are affected by the mutual interference effects between the airframe and nacelle. The static margin for longitudinal stability is also adversely changed. We develop a design approach in which the integrated geometry of airframe (HWB) and propulsion is accounted for simultaneously in a simple algebraic manner, via parameterization of the planform and airfoils at control sections of the wingbody. In this paper, we present the design of a 300-passenger transport that employs distributed electric fans for propulsion. The trim for stability is achieved through the use of the wingtip twist angle. The geometric shape variables are determined through the adjoint optimization method by minimizing the drag while subject to lift, pitch moment, and geometry constraints. The design results clearly show the influence on the aerodynamic characteristics of the installed nacelle and trimming for stability. A drag minimization with the trim constraint yields a reduction of 10 counts in the drag coefficient.

Nomenclature

ζ_{up}	=	Nondimensional CST *z* coordinates for airfoil upper surface
ζ_{low}	=	Nondimensional CST *z* coordinates for airfoil lower surface
η	=	Nondimensional *y* coordinates
η_{local}	=	Nondimensional local *y* coordinate
Λ_1	=	Sweep angle of the leading edge of the planform
Λ_2	=	Sweep angle of the outboard wing of the planform
λ_1	=	Coefficient representing the distance between the cabin body and the root chord of the outboard wing
λ_2	=	Coefficient representing the reach of the curved section of the leading edge of the outboard wing
λ_3	=	Coefficient representing the reach of the curved section of the trailing edge of the outboard wing
ζ_{un}	=	Nondimensional trailing edge thickness for the upper surface of the nth control airfoil on the aircraft
ζ_{ln}	=	Nondimensional trailing edge thickness for the lower surface of the nth control airfoil on the aircraft
ψ	=	Nondimensional CST *x* coordinates
A_u	=	CST optimization variable vector for the upper surface of the airfoil
A_l	=	CST optimization variable vector for the lower surface of the airfoil
b_{ow}	=	Span of the outboard wing
b	=	Span of the wing
b_2	=	Half span of the wing
c_{local}	=	Local chord length
$c_{r,cb}$	=	Root chord of the cabin body
$c_{r,ow}$	=	Root chord of the outboard wing
$c_{t,cb}$	=	Tip chord of the cabin body
$c_{t,ow}$	=	Tip chord of the outboard wing
h	=	Offset vector of the control airfoils for the aircraft
$h_{nacelle}$	=	Height of the nacelle as referenced from the surface of the aircraft
l_{cb}	=	Length of the cabin body
N	=	Bernstein polynomial order for CST airfoil generation of the aircraft
α	=	Angle of incidence
θ	=	Twist angle of the outboard wingtip
Δ	=	Increment
C_D	=	Drag coefficient
C_L	=	Lift coefficient
C_M	=	Moment coefficient
C_P	=	Pressure coefficient
F	=	Objective function
LE	=	Leading edge

[1] Aerospace Engineer, Inlets and Nozzles Branch (LTN). Senior Member AIAA

[2] *SAIC*, Aerospace Engineer. Senior Member AIAA; currently Professor at Kyung Hee University, Republic of Korea.

[3] *Vantage Partners, LLC*, Aerospace Engineer, Turbomachinery and Turboelectric Systems Branch (LTE). Senior Member AIAA

[4] Senior Technologist, Propulsion Division (LT). Fellow AIAA

N_1	=	Class function exponent for CST airfoil generation of the aircraft		MAC	=	Mean aerodynamic chord
N_2	=	Class function exponent for CST airfoil generation of the aircraft		*SM*	=	Static margin
w_{cb}	=	Width of the cabin body		*TE*	=	Trailing edge
x_{LE}	=	Leading edge position vector		*Q*	=	Flow variables
X	=	Dimensionalized CST x coordinates		$\boldsymbol{\beta}$	=	Design variables
Y	=	Dimensionalized CST y coordinates		*X*	=	Grid position
Z_{up}	=	Dimensionalized CST z coordinates for airfoil upper surface				
Z_{low}	=	Dimensionalized CST z coordinates for airfoil lower surface				

Subscript					
B	=	Baseline	*i*	=	Induced
c.g.	=	Center of gravity	*T*	=	Target
			Wt	=	Wing tip

I. Introduction

In this study, we performed the aerodynamic optimization of a hybrid wingbody (HWB) configuration that was integrated with an embedded distributed propulsion system. The hybrid wingbody, a.k.a. blended wingbody, is considered to have the potential to meet NASA's goals targeted for the 2030s for achieving reduction in fuel burn, noise, emission, and improvement cruise efficiency[1,2]. Embedded distributed propulsion concept utilizing ingested boundary layer offers benefits of low fan noise[3], noise shielding by a wide body[4], improved propulsive efficiency[5], and reduced ram and friction drags[1].

Unlike conventional tube-and-wing aircraft, HWB is a new technology with virtually no historical data available for actual aircraft. The development of a HWB aircraft involves unknowns and risks. Substantial challenges occur in the integration of the propulsion system with the airframe. Aerodynamic interferences and performance degradation are expected to be severe. Also the selection of engine types and the optimization of distributed engines is a new area of study. A comprehensive assessment of potential risks is given by Nickol[6]. Lyu et al.[7] point out the challenges in designing a HWB vehicle and review past studies done for design optimization of the HWB configuration. However, many of them are based on the clean HWB airframe, i.e., the aircraft without inlets/propulsion system. The embedded engines in a HWB vehicle are partially submerged in the boundary layer that develops from the leading edge towards the inlet. The boundary layer ingesting (BLI) inlet has several merits: reduced structural weight and noise, and improved propulsion efficiency by reducing form drag and wetted area. The BLI inlet has shortcomings of higher flow distortion and lower pressure recovery[8,9]. Flow separation can occur in the diffusing inlet because of the low momentum BLI flow or in the S-bend of the offset inlet, resulting in insufficient air supply to the fan face.[10] The installation of the nacelle has been shown to significantly degrade the aerodynamic efficiency of the clean wing configuration. For example, a separated flow region on the upper surface of a nacelle that housed an array of fans for the N3-X configuration, as seen in Fig. 1[11]. Similar phenomenon was also observed for other propulsion concepts on the N3-X and flow separation still existed, although a reduction in the size was achieved after optimizing the nacelle shape[12,13]. It has become abundantly clear in our previous studies[11-13] that it is extremely difficult (and inefficient) to achieve a desirable aerodynamic efficiency when the airframe and propulsion system are handled sequentially in a decoupled manner for a highly integrated configuration. This has motivated us to develop a design approach that includes both the airframe and propulsion systems at once at the outset of aerodynamic design of the aircraft. This implies that it is necessary to have a general and relatively easy procedure to describe the geometry of the integrated configuration. We adopt the parameterization method proposed by Kulfan[14] to achieve this purpose. Since the HWB considered does not have a horizontal tail to stabilize the aircraft, the wing has to take over the tail's functions in providing stability and control. In Ref. 1, trim is listed as one of design requirements for an integrated HWB airplane. A negative pitching moment derivative with respect to lift and a positive pitching moment coefficient at zero lift are two principal conditions for an airplane to be longitudinally static stable and trimmable. A negative pitching can be obtained by adjusting the position of the center of gravity with respect to the aerodynamic center and a positive pitching can be achieved by employing washout along the wingspan and sweeping the wing aft[15]. To achieve either purpose, the aerodynamic forces and moment over the complete HWB configuration must be properly designed[7,16].

The main objective of the present HWB work is to develop a approach that optimizes aerodynamic performance under the stability requirement for a complete configuration that includes simultaneously the airframe and propulsion systems in the preliminary design. The intent of this paper is to: (1) present the capability for incorporating both the airframe and propulsion geometries simultaneously in a simple and efficient fashion, (2) perform aerodynamic trim to achieve an optimal design, and (3) provide a detailed analysis comparing performances of the baseline and optimized vehicles. The present paper is organized as follows. Section II describes the parameterization method used for defining the integrated HWB geometry. Section III describes the formulation of the optimization problem, trimming for stability, and numerical tools. CFD aerodynamic analysis and the resulting optimal designs are given in Section IV and finally concluding remarks are made in Section V.

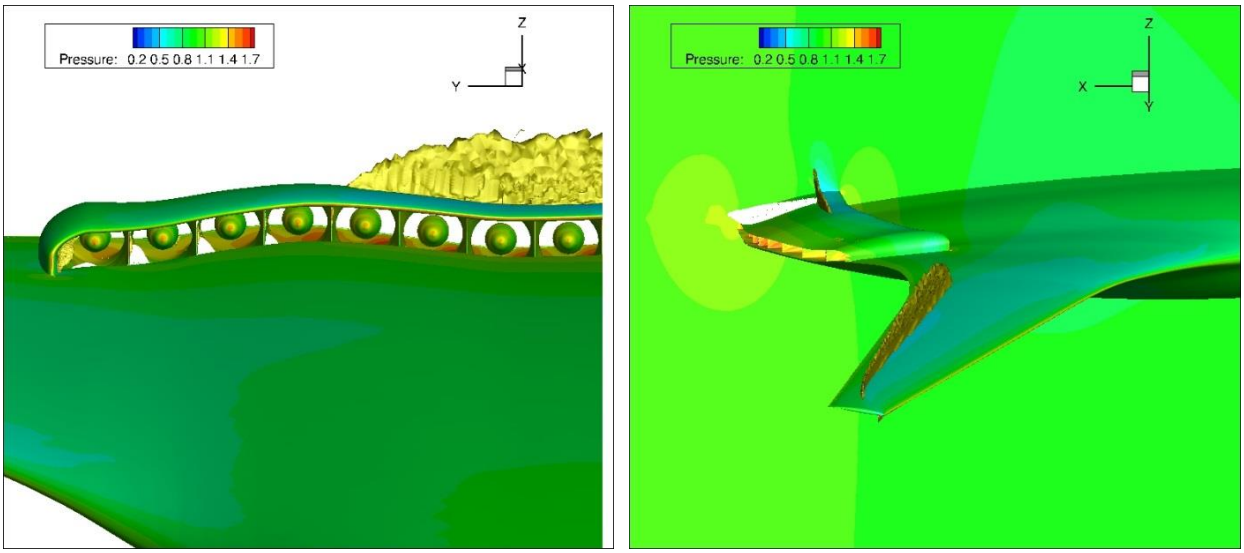

Figure 1: Previous result of the Navier-Stokes simulation of the N3-X[11]; there are 8 mail-slot fan-propulsors installed on each side from the symmetric plane. Yellow contours denote the separated flow regions, notably on the upper surface of the nacelle and trailing edge of the outboard wing section.

II. HWB Geometry and Parameterization

To carry out optimization for aerodynamic performance of an aircraft, it is necessary to represent its geometry with a set of parameters (design variables) such that they can be succinctly manipulated in a simple and efficient manner to achieve design objectives. The Class function Shape function Transformation (CST)[14], a non-dimensional airfoil/wing generation method, is shown in Ref. 17 to be capable of creating a variety of geometries and hence adopted to construct the HWB airframe-propulsion configuration. In this section, we describe how we accomplish the design parameterization procedure for representing a complete HWB configuration that is composed of the airframe and propulsion geometries. Additional details may be found in our previous paper[15]. Geometric requirements such as internal cabin and cargo hold layouts etc. are imposed to set the bounds of the values of parameters.

Our geometry modeler consists of four steps: (1) generation of HWB airframe planform, (2) generation of control airfoils at specified spanwise sections, (3) generation of interpolated airfoils based on the control airfoils, and (4) generation of the nacelle geometry. The first task is achieved by employing piecewise polynomials through a set of specified control points. The second task is the backbone for completing a 3D HWB through the use of the CST method at a small number of key sections. The third task is to create interpolated airfoils in order to complete a smooth aerodynamic body. The final step is to build one or multiple nacelle on top of the clean wingbody that is obtained through step (1), (2), and (3). In what follows, we shall describe each of these tasks in sequence.

A. Planform

The planform is the two-dimensional shadow (outline) of the aircraft when viewed directly from above the craft. Shown in Fig. 2 is a typical planform of a HWB vehicle and denoted are the set of geometrical parameters involved in defining its shape. This formulation is a slight modification from the one by Laughlin[17]. To construct the leading and trailing edges and wing tips of the HWB, we use 10 control points, (x_1,y_1) to (x_{10},y_{10}) as labeled in Fig. 2. The points are determined by solving two systems of linear equations via introduction of twelve parameters: $c_{r,cb}$, $c_{t,cb}$, $c_{r,ow}$, $c_{t,ow}$, w_{cb}, l_{cb}, b_{ow}, Λ_1, Λ_2, λ_1, λ_2, and λ_3. These parameters are our planform design variables. They are intuitive and bear physical and geometrical meaning. Some are based on the sizing requirement from a specified mission, such as the first seven parameters, the remaining parameters control the sweep angles of the nose and outboard wing section, and the blending (curvature) between the body and wing sections. Then a combination of cubic and linear polynomials is used to define the inboard and outboard sections respectively, using the already-solved control points. Details can be found in Ref. 18.

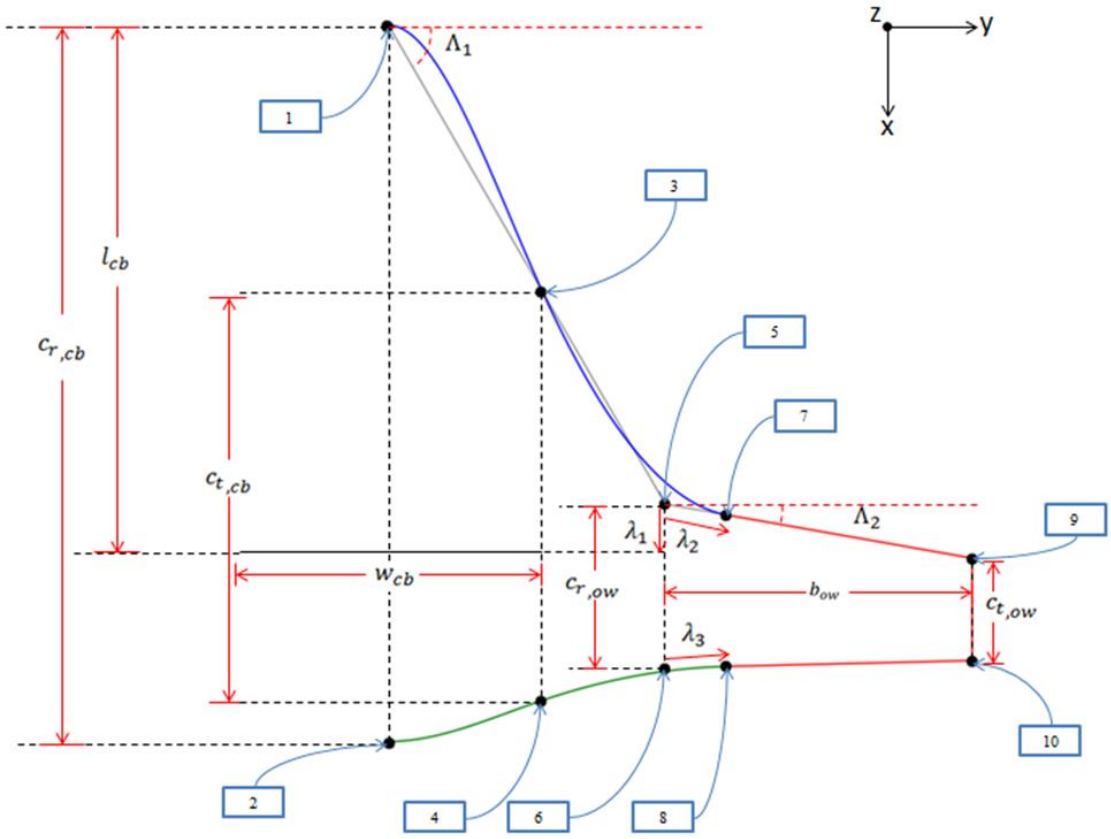

Figure 2: Planform definition of a hybrid wingbody configuration.

B. Control Airfoils

The first step in generating the complete 3D geometry of the wingbody-propulsion configuration is the creation of the clean (i.e., sans propulsion/nacelle) wingbody. This is begun with the generation of a series of airfoil shapes at various control planes (y=constant), hence they are named control airfoils. The airfoils are described using the CST[14] method with a universal formula. In the CST method, a non-dimensional airfoil (local) x-coordinate, ψ, is employed so that the formula is common for all control airfoil sections. The airfoil has values $\psi = 0$ at the leading edge and $\psi = 1$ at the trailing edge. For a cambered airfoil, the upper and lower surfaces of the airfoil are defined with the same formula, but different sets of parameters. The non-dimensional z-coordinates, ζ_{up} and ζ_{low}, respectively, for the upper and lower curves of a control airfoil, are defined as:

$$\zeta_{up} = \psi^{N_1}(1-\psi)^{N_2}\sum_{i=0}^{N}\left(A_{u_i}\left(\frac{N!}{i!\,(N-i)!}\right)\psi^i(1-\psi)^{(N-i)}\right) + \psi\,\xi_u \tag{1}$$

$$\zeta_{low} = \psi^{N_1}(1-\psi)^{N_2}\sum_{i=0}^{N}\left(A_{l_i}\left(\frac{N!}{i!\,(N-i)!}\right)\psi^i(1-\psi)^{(N-i)}\right) + \psi\xi_l \tag{2}$$

where A_{u_i} and A_{l_i} refer to the i^{th} value of the design parameter vector for the upper and lower surfaces of the section airfoil. The ξ_u and ξ_l can be used to define the (non-dimensional) trailing-edge thickness and twist. The condition $\xi_u = \xi_l \neq 0$ gives a zero trailing edge thickness, but with a twist (rotation) relative to the leading edge. For the HWB configuration considered here, we set $N_1 = 0.5, N_2 = 1$, and $N = 7$. As the initial sectional airfoil shape in this study, the sectional shapes of the N3-X configuration[12] is extracted and fitted by the CST method by gradient-based optimization. Figure 3 shows the results for the curve fitting for airfoils at 0%, 30%, 70%, and 100% semi-span sections of the N3-X airframe.

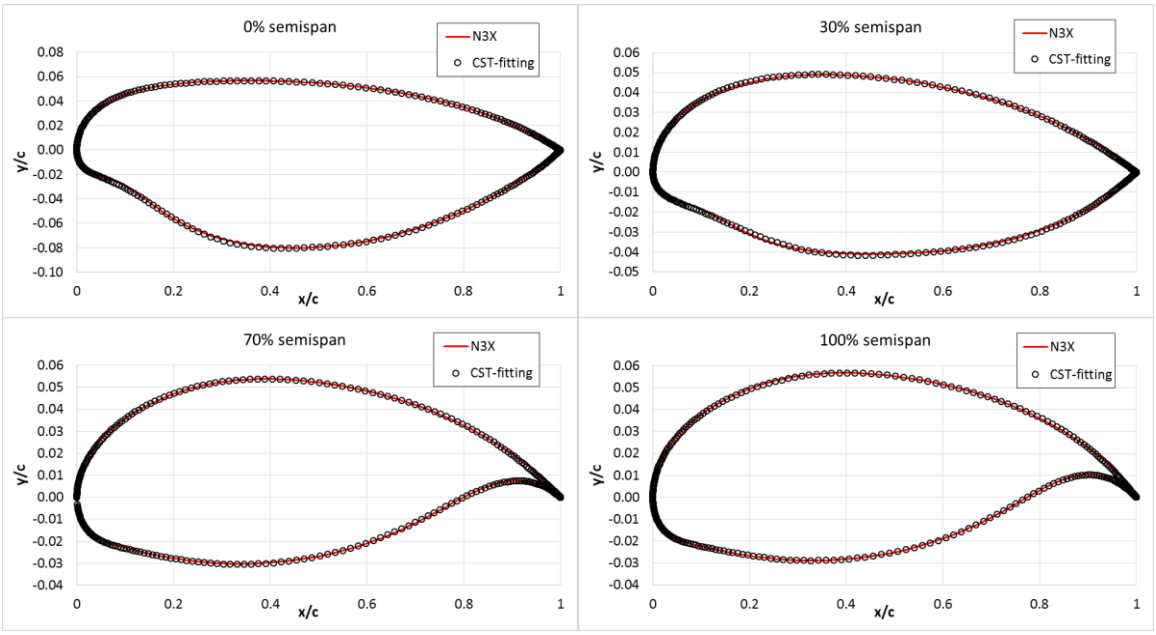

Figure 3: CST Control Airfoils for the Hybrid Wing Body Aircraft

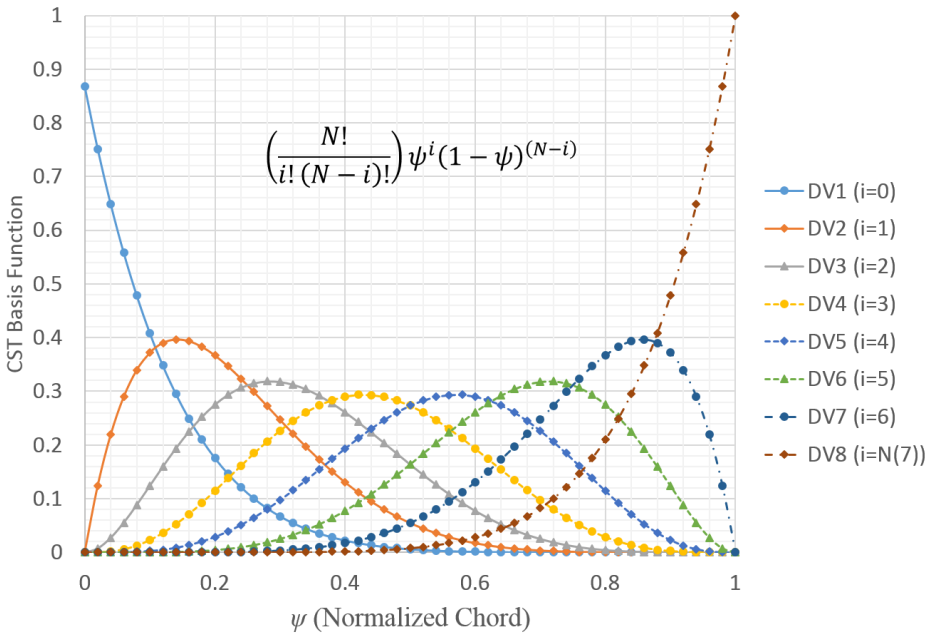

Figure 4. A showcase of CST basis functions used in creating control airfoils.

To generate the clean wingbody, four control sectional airfoils are placed along the spanwise direction at y_1, y_3, y_7 and y_9, from root to wingtip respectively. These typical control airfoil sections for a complete aircraft, after mirroring three off-center sections to the other half of the aircraft, are indicated in black color as shown in Fig. 5 (a) and (b). Specifically, Fig. 3 exhibits the four control airfoil sections used in this N3-X study. The CST $N + 1$ Bernstein basis polynomials of degree N, as mathematically expressed in Eqs. (1) and (2), are plotted against the non-dimensional x-coordinate, ψ , in Fig. 4. Obviously, the summation of all eight basis polynomials yields great versatility in representing various airfoils from the 10% to 80% chord, but somehow may be short of control points in two separate zones. They are from the leading edge to 10% chord and 90% chord on to the trailing edge.

C. Interpolated Airfoils and Volume Requirement

At any given spanwise location, the sectional airfoil must have its own set of unique CST parameters (i.e. $A_{u_i}, A_{l_i}, i = 0, N$), twist, and z-offset values. A complete loft (volume) of the aircraft is obtained by interpolating two neighboring control airfoils in the spanwise direction. In other words, these sets of the CST parameters are interpolated between two closest control airfoil sections, based on a local non-dimensional *y* coordinate, $\eta_{local} \in [0,1]$, with $\eta_{local} = 0$ corresponding to the control section closer to the root chord and $\eta_{local} = 1$ at the other control section. Hence, the following formulas are used to determine the CST parameters at any interpolated section

$$A_u = A_{0,u} + \left(A_{1,u} - A_{0,u}\right)F(\eta_{local}), \tag{3}$$

$$A_l = A_{0,l} + \left(A_{1,l} - A_{0,l}\right)F(\eta_{local}), \tag{4}$$

where $A_{0,u/l} = A_{u/l}(\eta = 0), A_{1,u/l} = A_{u/l}(\eta = 1)$, and function F can be defined as a linear function (F = η_{local}), or a cubic function (F = ${\eta_{local}}^2(3 - 2\eta_{local})$). The cubic function is used here for smoothness.

After the above airfoil generation, these non-dimensional sectional airfoils need to be dimensionalized to get the correct physical scales of the aircraft, based on planform location parameters. The local chord length c_{local} is used for the *x* and *z* coordinates and the half span *b* is used for the *y* (spanwise) coordinates. Furthermore, the *x* and *z* coordinates each have an offset term added to them. The x coordinates have an offset $x_{LE}(Y)$ corresponding to the leading edge position of each respective sectional airfoil; this offset is a function of the planform. The *z* coordinates have an offset $h(Y)$ that can be utilized to create a dihedral or anhedral wing. The dimensionalizing procedure is given in Eqs. (5)-(8).

$$Y = \eta b \tag{5}$$

$$X = \psi c_{local} + x_{LE}(Y) \tag{6}$$

$$Z_{up} = \zeta_{up} c_{local} + h(Y) \tag{7}$$

$$Z_{low} = \zeta_{low} c_{local} + h(Y) \tag{8}$$

A front view and isometric view of the clean wingbody is shown in Fig. 5, after creating sufficient interpolated airfoil section. Now the task of generating a clean wingbody is completed.

(a) Front view of a clean hybrid wingbody aircraft.

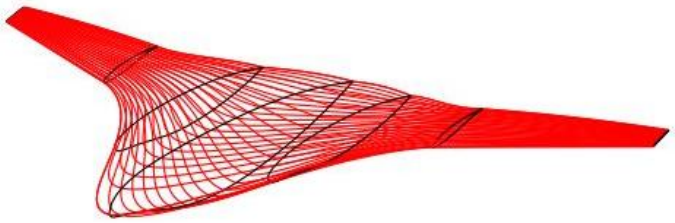

(b) Isometric view of a clean hybrid wingbody aircraft.

Figure 5: Interpolation of the airframe sectional shapes from four design sections for half HWB geometry; these four are defined in subsection C and shown in Fig. 3.

The HWB planform and sectional shapes must provide a sufficient interior volume that can accommodate payload requirement set by the mission, such as the passengers cabin and cargo hold, along with internal structures. For our study, we adopt the layout of cabin and cargo space suggested by Nickol[6] for a 301-passengers aircraft, which is

depicted in Fig. 6. Based on this layout, we generated a volumetric model of cabin and cargo hold, which in turn leads to adjustment of design parameters such as the airframe planform and sectional airfoil thicknesses, so that the required cabin and cargo space can fit inside the aircraft. The result is shown in Fig. 7, with the cabin and cargo blocks highlighted.

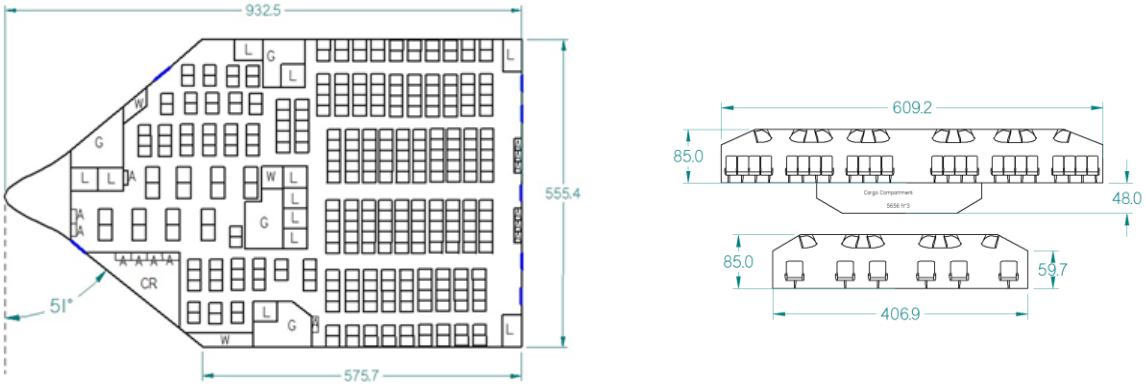

(a) Top view of cabin layout. **(b) Front view of cabin and cargo hold.**

Figure 6: HWB Cabin layout design for 301 passengers.[6]

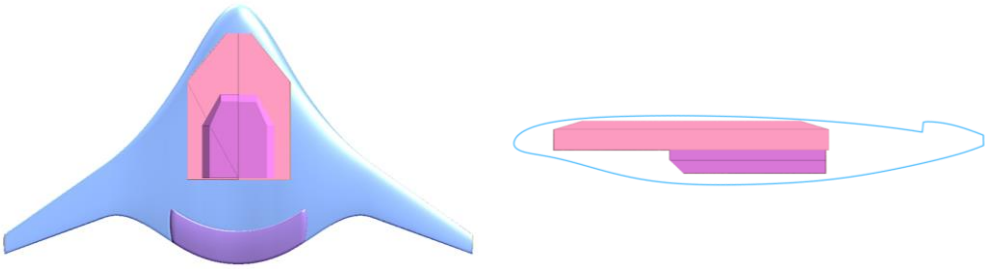

Figure 7: HWB configuration and cabin/cargo hold positioned in the airframe.

It is of value to be able to locate the Cartesian coordinates of any given point on the surface of the aircraft. The ability to do that efficiently and accurately is crucial in such tasks as positioning external aircraft components and writing geometry files to be used in aerodynamic analysis. Due to the method describe above, it is actually quite a simple task to determine the z coordinates corresponding to any given planform (x, y) coordinate. When a y coordinate is specified, the two control airfoils that bound the point are identified immediately, based on the local non-dimensional y coordinate η. Since ψ is independent of the span, an interpolated airfoil can be generated. Once the interpolated airfoil is generated and properly dimensionalized, the given x coordinate can be pinpointed along the chord of the interpolated airfoil. Using this x coordinate, the upper and lower z coordinates can be easily determined.

D. Nacelle

After the clean wingbody geometry is generated, the final step in generating the geometry of the complete HWB aircraft is to add the nacelle. The propulsion system considered for the current N3X configuration uses an array of distributed electric fans to provide thrust. The fans are housed in a narrow, wide span nacelle, each placed inside a slot, thus also dubbed the "mailslot" nacelle, as seen in Fig. 8. The nacelle is located on the upper rear surface of the aircraft. The HWB aircraft is hereafter denoted as N3X-DEP, referring to NASA's third generation (in the time frame of the 2030s) concept with distributed electrical propulsion.

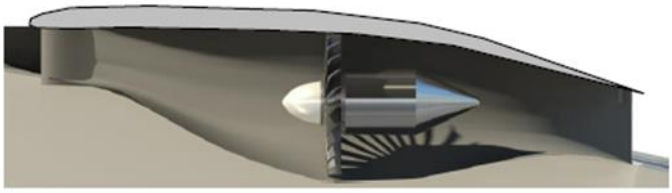

Figure 8: A fan-propulsor housed in the mail-slot nacelle geometry in N3X-DEP.

The nacelle geometry was first generated with defined leading edge and trailing edge profiles. Translational movements can be made in the chord-wise direction for any given nacelle planform on the airframe. Also, rotational movements for each sectional airfoil of the nacelle are required so the nacelle is aligned with the local slope of the airframe upper surface at the installation location. In this study, it is assumed that the nacelle has constant chord length in the spanwise direction, and the nacelle trailing edge follows the trailing edge of the airframe. This assumption can be easily changed when needed.

In the study presented here the nacelle has a simplified geometry with only a single flow passage, see Fig. 9, instead of multiple internal slots[12]. This simplified nacelle geometry gives fast turnaround for design optimization while including interference effects of the propulsion geometry on the airframe aerodynamics. It is noted that the single passage is not a flow-through passage, but terminated by a boundary plane at fan face across which a fan pressure ratio is imposed to represent an estimate of energy input by the fan. This corrected pressure condition is then specified at the nacelle exit plane. These two planes are depicted in Fig. 9.

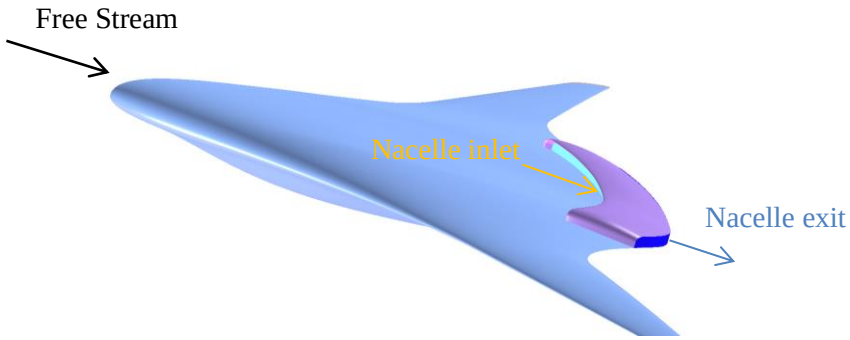

Figure 9: Mail-slot nacelle geometry (side view: flow goes from left to right and the opening section is on the HWB symmetry plane).

The nacelle surface follows the contour of the airframe surface and sits on top of the upper surface. Therefore, the nacelle height $h_{nacelle}$ is a function of the upper surface. The nacelle geometry consists of the top cover, the legs and rounded corners. The corner can be parameterized to yield a smooth outline of the inner and outer surfaces; here we use an ellipse. Figure 10 depicts the front view of the mail slot nacelle installed on the airframe, showing the horizontal, elliptical corner and vertical sections of the nacelle. The cross section of the mail slot nacelle is also airfoil-shaped for aerodynamic efficiency. Therefore, the cross section of the nacelle can be created also using CST as described above.

III. Optimization Problem Formulation

In our previous study[13], drag minimization was performed by deforming the HWB airframe and nacelle cowl while the lift and twist were hold constant. A noticeable change in the outer cowl shape was observed, which resulted in a reduction of the strength of shock. Since the aerodynamic loading is changed after the nacelle is installed, it affects all aerodynamic performance metrics, which include the lift, drag, and moment coefficients. In this study, we shall focus on trimming in relation to stability, specifically using a spanwise washout to trim the integrated HWB. Four twist angles are specified at four sections from root to wingtip and were chosen as design variables. Among them, a quadratic interpolation is used for inboard sections and a linear function used between the last two in the outboard. The outboard wingtip twist angle especially plays a significant role in trimming HWB aircraft. An interesting question is posed in this study to answer: is it possible, using the wing tip twist, to generate a pitching moment so that the

overall moments about the center of gravity is zero? Therefore, the wingtip twist angle is used here as an input variable to derive the trim constraint while the rest of twist angles can be determined by the optimizer. In this section, firstly the specified objective function, constraints, and relevant design variables are described and formulated to satisfy trim condition and a target lift coefficient. Secondly, the static margin is introduced to maintain a positive static stability requirement when the HWB in trim is subjected to a disturbance that changes the incidence. Then the optimization method used in this work is described and followed by a description of the CFD tool employed.

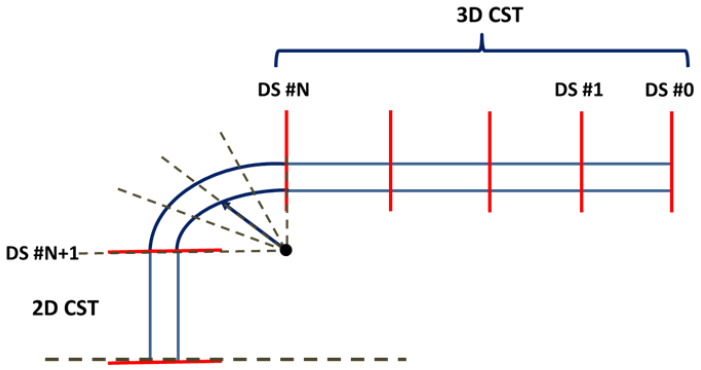

(a) Definition of nacelle cowl shape with N+1 design sections (DS)

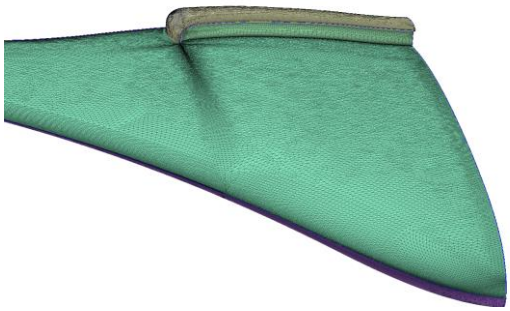

(b) Front view of the discretized single passage mail slot nacelle integrated with the HWB; purple color indicates the lower surface of the HWB

Figure 10: Front view of mail slot nacelle, showing horizontal, corner, and vertical sections of the nacelle.

A. Definition of Objective Function

The design objective of the present study is to minimize the drag while ensuring longitudinal stability. The problem can be stated as follows:

$$\text{Minimize:} \quad C_D \tag{9}$$

$$\text{Subject to: } C_L = C_{L_T},\ C_M = C_{M_T} = 0,\ \textit{Specified SM} \tag{10}$$

$$R_{LE,nacelle} \geq R_{LE,baseline\ nacelle} \tag{11}$$

$$(t/c)_{max} \geq (t/c)_{max,baseline}\ \textit{for each design section} \tag{12}$$

where C_{L_T} and C_{M_T} are the target lift and moment coefficients (hereafter the moment coefficient is evaluated with respect to the center of gravity unless specified otherwise). The baseline cruise lift coefficient is chosen as the target value; SM is the static margin for longitudinal static stability. To achieve the constraints on C_L and C_M, we first trim the aircraft by adjusting incidence angle α and twist angle at wingtip θ_{wt}. The corresponding drag coefficient for this adjustment is estimated by the first order Taylor series:

$$C_D = C_{D_i} + \frac{\partial C_D}{\partial \alpha}\Delta\alpha + \frac{\partial C_D}{\partial \theta_{wt}}\Delta\theta_{wt}$$
$$= C_{D_i} + C_{D_\alpha}\Delta\alpha + C_{D_\theta}\Delta\theta_{wt}, \quad (13)$$

where C_{D_i} is the drag coefficient at the beginning of the i^{th} optimization design cycle, $\Delta\alpha$ and $\Delta\theta$ are the required variations in angle of attack and wing tip twist angle that satisfy the constraints, Eq. (10). The derivatives C_{D_α} and C_{D_θ}, with respect to α and θ_{wt}, can be obtained by finite differencing through CFD calculations. Moreover, the amounts of $\Delta\alpha$ and $\Delta\theta_{wt}$ can be related to changes in C_L and C_M from the target values as:

$$\begin{pmatrix}\Delta C_L \\ \Delta C_M\end{pmatrix} = \begin{pmatrix}C_{L_\alpha} & C_{L_\theta} \\ C_{M_\alpha} & C_{M_\theta}\end{pmatrix}\begin{pmatrix}\Delta\alpha \\ \Delta\theta_{wt}\end{pmatrix}, \quad (14)$$

where $\Delta C_L = C_{L_T} - C_L$ and $\Delta C_M = C_{M_T} - C_M$. The derivatives C_{L_α}, C_{L_θ}, C_{M_α}, C_{M_θ} are again obtained by finite differencing of CFD solutions. Hence, the required $\Delta\alpha$ and $\Delta\theta$ at trimmed condition can be obtained by solving the above equations with imposed constraints: C_{L_T} is the baseline cruise lift and $C_{M_T} = 0$. Hence,

$$\begin{pmatrix}\Delta\alpha \\ \Delta\theta_{wt}\end{pmatrix} = \begin{pmatrix}C_{L_\alpha} & C_{L_\theta} \\ C_{M_\alpha} & C_{M_\theta}\end{pmatrix}^{-1}\begin{pmatrix}\Delta C_L \\ -C_M\end{pmatrix} \quad (15)$$

This is then substituted back in Eq. (13) to get the C_D for the trimmed configuration for the design with the current design variables. The moment coefficient is evaluated with respect to a specified location. In our case it is the center of gravity (CG), which is varied by the required static margin (SM), as described below.

B. Calculation of the Aerodynamic Center for Trim and Stability

To determine the static trim conditions in the integrated HWB design, two principal factors influence longitudinal stability: (1) washout angle along the wing span, and (2) position of the center of gravity (CG) relative to the neutral point, also is known as the SM. The former is a feature in wing design which deliberately modifies the spanwise lift distribution to reduce the induced drag and to prevent the tip stall from occurring before the root stall. The latter will be briefly described below. In the absence of a tail to balance stability, the CG has to be positioned forward of the neutral point[17] of the wing to create a moment arm for a necessary pitching moment. Conventionally, the SM is defined as the distance between the CG and the neutral point defined as the center of gravity location for which the vehicle is in neutral pitch stability[19]. Thus, the static margin is also the distance between the CG and the aerodynamic center (AC) for the HWB. The CG is determined by the design of the aircraft and can be changed by the cargo, passengers, fuel etc. while the AC is not. In this study, we fix the SM and calculate the required twist angle at the wing tip, θ_{wt}, to satisfy the trim condition. For convenience, the AC is determined first in this study for it can be easily determined by C_M values from the flow solver, as described below.

Assuming the momentum coefficient C_M is a linear function of the angle of attack, the C_M at the aerodynamic center is found by using known values of C_M at the leading edge and the trailing edge of the mean aerodynamic chord (MAC) for two separate angle-of-attack (AOA), respectively, shown by lines in silver and blue colors of Fig.11. The values of C_M on the silver and blue lines at two clustered points (i.e. at 0.1 degree step size) are obtained from CFD solutions. The intersection of the two lines yields the location of AC, at which the moment coefficient $C_{M_{a.c.}}$ remains independent of lift coefficient (or angle of attack), which is confirmed by the yellow line in Fig.11. Consequently, CG can be located from the known location of AC and the imposed static margin constraint, Eq. (10), for a longitudinally stable is satisfied. The required pitch moment at CG in Eq. (15) is determined accordingly. The static margin can be calculated as the ratio of the moment and lift derivatives with respect to AOA. Both C_{L_α} and C_{M_α} are calculated using the finite differences with an angle of attack step size of 0.1 degree, as described previously.

C. Aerodynamic Shape Optimization by the Adjoint Method

The next step is to follow the optimization procedure, once the objective function C_D is evaluated and the constraints satisfied. The gradient-based adjoint method[20] is adopted for optimization for this study because the computation cost is essentially independent of the number of design variables, although it has the shortcoming of finding only a local optimal solution. The method is rather standard and its technical details are omitted here. Based

on the sensitivity derivative of the objective function F with respect to design variables, the optimization code is then tasked to search the necessary changes in the design space subject to the geometrical constraints, e.g., Eqs. (11) and (12). The process is repeated until a minimum trimmed C_D is obtained; the required iteration number is normally less than 10. However, we note that scaling is used to normalize the design variables and to enhance the efficiency of optimization. Here only the twist angles of the HWB design airfoil sections, excluding the wingtip twist angle, are scaled before using the Broyden-Fletcher-Goldfarb-Shanno[21] variable metric method.

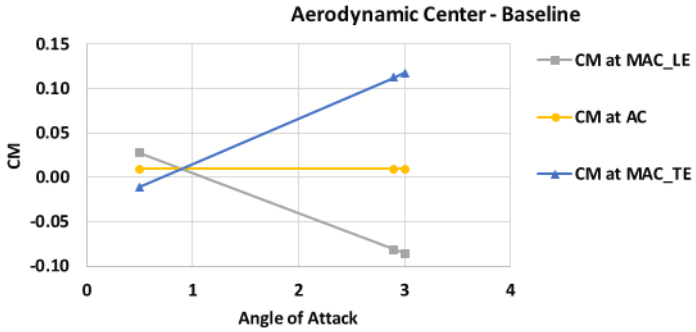

Figure 11: The determination of the aerodynamic center and its associated coefficient of moment by finite differencing.

D. CFD tool

Goflow, a three-dimensional unstructured mesh Navier-Stokes flow solver, is used for flow simulation, but only inviscid solutions are calculated for its computing efficiency and for demonstration purpose of the current capability of designing a complex integrated geometry of a HWB configuration. The flow going through the propulsion passage is represented by a simple block model, in which the computation domain for the engine flow is terminated at the fan face by setting a proper static back pressure at the fan face boundary. A fan pressure ratio of 1.3, was determined from the system study[9] for the propulsor to provide sufficient thrust for the aircraft and is imposed to provide the condition for the engine exit flow at the nacelle outlet. In addition, the flow at the nacelle outlet is assumed choked, i.e., setting the Mach number to unity.

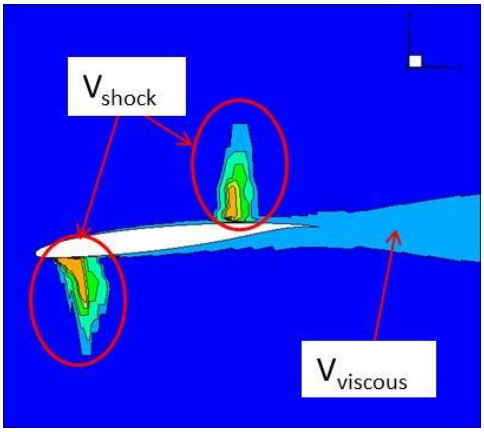

Figure 12: Domain decomposition for drag breakdown in the far-field approach.

A reliable drag prediction is critical for the aerodynamic shape design and optimization. A conventional approach for drag force calculation on aerodynamic configurations is to directly integrate forces acting on body surfaces. This "near field" approach, although easy and straightforward to implement, can incur spurious drag caused by errors from numerical scheme and quality of computational mesh. Moreover, it does not provide in-depth information on the origin of drag force and is difficult to make corrections. On the other hand, the "far-field" (control volume) approach is based on a far-field integration of irreversible entropy drag (viscous and wave drag) and reversible induced drag components.[22] The far-field approach can give a breakdown of total drag into viscous, wave and induced drag terms. In addition it also specifies spatial origin of each entropy drag component. Another method, called the mid-field

method, is a further improvement from the far-field method.[23] It computes drag components from volume integration around the aircraft and can be decomposed into wave, form, induced and spurious drag. The ability to isolate the spurious entropy produced by numerical diffusion makes the mid-field method the most accurate among all three approaches in drag prediction.[23] Moreover, the drag strength and its spatial position can be visualized through the mid-field method, same as the far-field method. In this study, a mid-field drag decomposition code was developed following the approach in Ref. 23. Figure 12 shows an example of computational domain decomposition for drag breakdown, where V_{shock} represents volume of wave drag domain, and $V_{viscous}$ means volume of viscous drag domain.

IV. HWB Design Results and Performance Analysis

The baseline geometry was generated by the HWB parameterization method described in the section II. The vehicle surface was composed of structure meshes, from which an unstructured mesh was generated on the same surface and volume mesh in the defined computational domain. For a fast turnaround of flow simulations during design optimization process of the HWB airplane, any geometric change from the baseline structured grid should be transferred to the unstructured computational surface grid. When the surface deformation was defined, the volume mesh points were deformed accordingly using the spring analogy approach. Thus, once a computational mesh is generated, it can be easily deformed for another set of geometric parameters. The baseline airframe, the HWB N3X-DEP for 301 passengers, has the planform of a span of 213 ft., a root chord length of 118 ft., the leading edge sweep angle of center body of 51 degrees and a reference area of 5028 ft^2. The volume of the cargo hold is kept larger than the required volume of 5656 ft^3 (equivalent to the cargo hold volume of Boeing 777-200LR). The nominal cruise condition used in this study is at Mach 0.84, altitude 35k ft., and angle of attack of 3 degrees. The number of design variables was 141 in total: 12 variables for planform, 64 design variables for the four HWB airframe sectional airfoils, 9 spanwise twists, and 56 for the nacelle.

A. Shape Design of the Clean and Integrated HWB Configuration Design

Optimization techniques for changing geometric shape locally have been proven useful in improving HWB performance, for example by reducing/eliminating shock wave, thus resulting in a significant drag reduction[24]. However, the aerodynamic characteristics are changed once the nacelle is installed. Reference 11 gives details regarding the influence of installed nacelles on the clean airframe performance, noticeably supersonic pockets are generated on the nacelle outer surface and flow separations occur outside and inside of nacelle. Also, the underbody flow field at the trailing edge can be disturbed by the engine exhaust. To accomplish aerodynamic shape design with constraints of targeted aerodynamic performance, trim and longitudinal static stability, the procedure described in the section III was employed for both the clean and the integrated HWB configurations. All results presented in the following were trimmed and positive static margin was satisfied. Computational surface meshes with and without a nacelle are shown in Fig. 13.

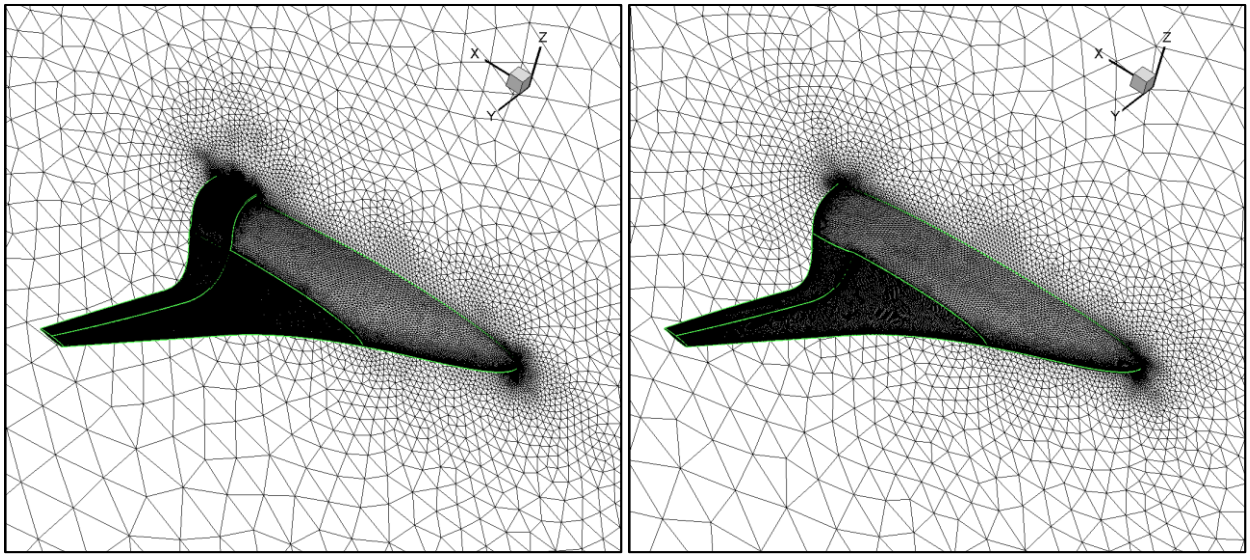

Figure 13: Computational meshes for the HWB with and without nacelle.

Figure 14 summarizes the design optimization conducted on the clean wing configuration, optimized design on the right and baseline on the left. Four pressure coefficient C_P plots (a), (b), (c) and (d) at root, 30%, 60%, and 95% chord respectively are arranged in clockwise direction, the blue line indicating the baseline and red for its optimized results. The root section, Fig.14-(a), doesn't show any notable change while the outboard wing sections seen in Figs. 14-(c) and (d) are fundamentally changed. Outboard sections had lower twist angles (pitch up) thus, aft-loaded supercritical airfoils turned into front loaded airfoils. The positive camber at trailing edge (from 90%c to TE) at the 60%b_2 (b_2 being the half span) section becomes slightly negative. Through these change, the negative loading at LE of outboard sections are reduced significantly, and the strong shock at the upper wing surface is almost removed. The center of gravity (X_{CG}) moves to 0.3673c from 0.3821c since the optimized wing is more front loaded relative to the baseline wing.

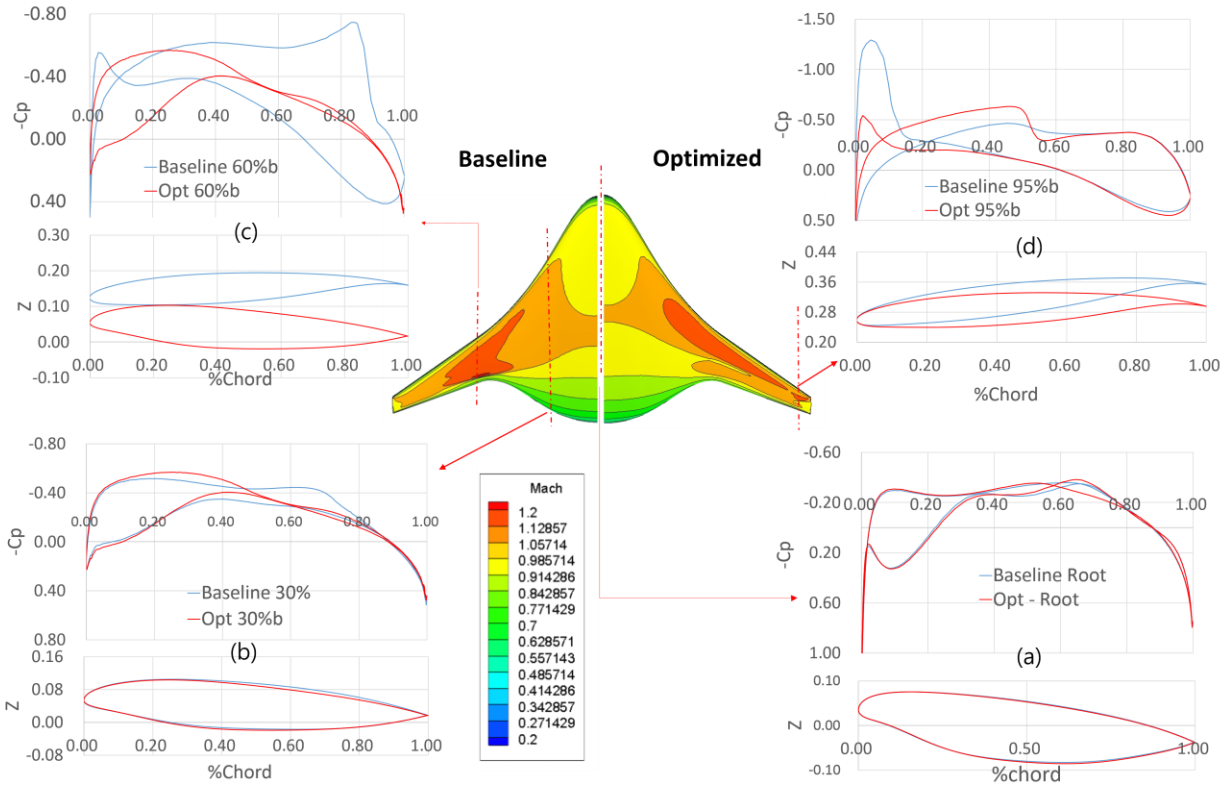

Figure 14. Optimized geometry comparison, Clean Wing Baseline (Left) vs Optimized (Right). Color blue and red represent the baseline and the optimized design respectively in plots of the sectional pressure coefficient (C_p) distribution and sectional shape at sections (a)-(d).

Optimized designs of the clean and integrated configurations are compared in Fig. 15, including the surface Mach contours, the sectional geometry at the root, the pressure distribution on the symmetry plane, and spanwise lift distribution. The C_p curve at the wing root, Fig. 15-(a), shows a larger negative loading in the 60%~90% chord than the clean wingbody, while from 90% chord to TE a high positive loading is found. The change seems to originate from the trim constraint to compensate additional lift from nacelle. Figure 15-(b) shows the spanwise loading follows nearly the ideal elliptic distribution, departs noticeably in the inboard region between the root and 40% of the half span, which may explain the increase in the total lift coefficient. The clean wing case follows more or less the elliptic distribution in Fig. 15-(c). This difference in spanwise lift distribution may stem from the fact that flow expansion and shock structure exist on the cowl upper surface between 0% and 20% span. Figure 15-(d) shows that the optimization dictates the twist angle at the root section to pitch up and the aft-body to become slender in the nacelle-wing configuration. Moreover, the induced drag $C_{D_{ind}}$, calculated using the mid-field drag breakdown method, has a dramatic increase of 19 counts.

Table 1 lists values of aerodynamic characteristics for both configurations. Improvements were observed in reducing wave and induced drags by optimization in each configuration. The wave drag of 3.3 counts for the baseline clean configuration is reduced to 0.4 counts by optimization, the induced drag reduced by about 3 counts, and the lift

to drag ratio increased from 52.3 to 67.6. However, for the integrated configuration, the improvement in induced and wave drags by optimization is limited, about 1 to 2 counts, the cowl wave drag however is nearly eliminated, and the lift to drag ratio is improved from 38.2 to 45.4. More details of nacelle effects in loading and trim constraint will be discussed in the following section. Hence, we conclude that the nacelle (or propulsion system) installation affects the aerodynamic characteristics remarkably for the HWB configuration considered.

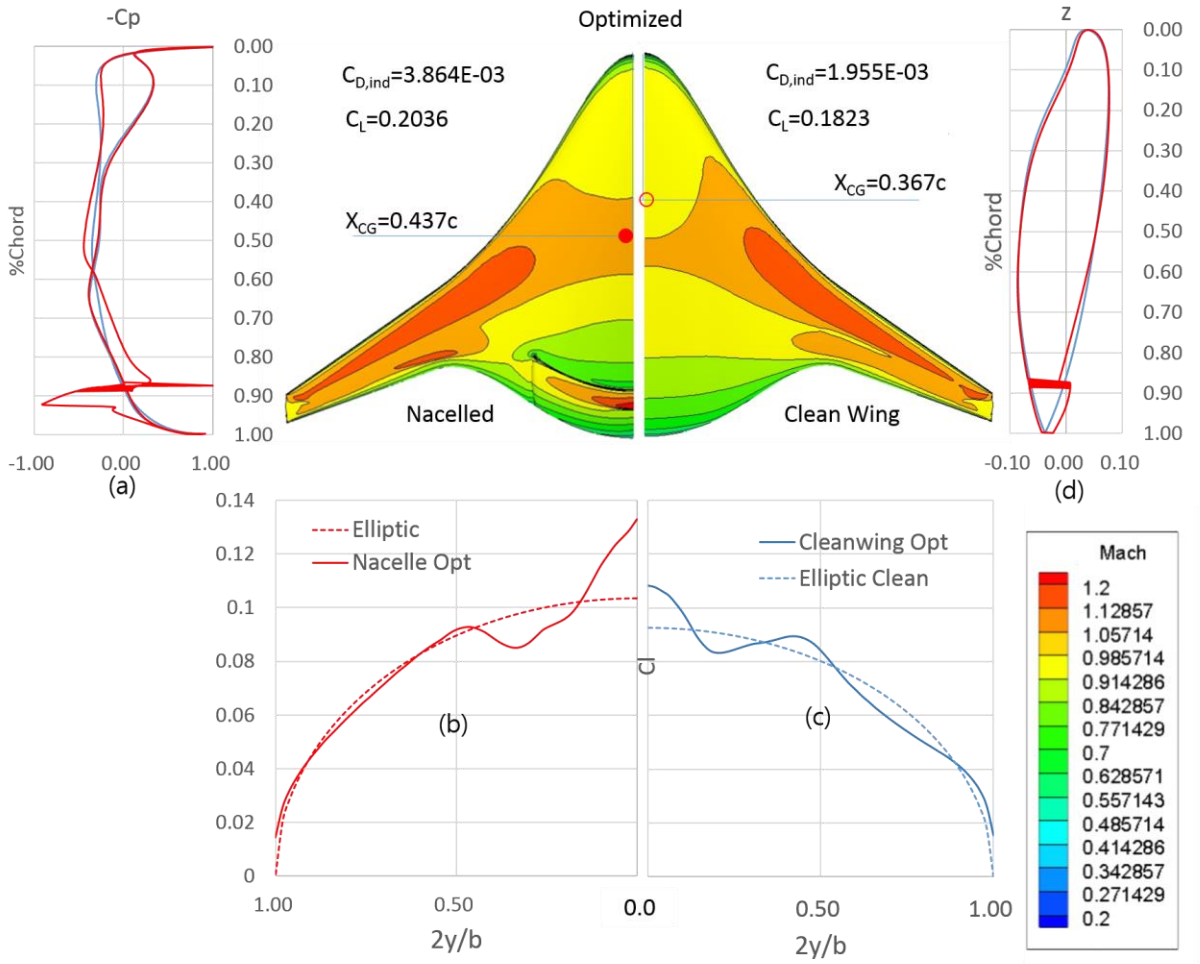

Figure 15. Comparison of optimized results for the clean wingbody (blue) and nacelle-wingbody (red) configurations.

Recognizing the need to couple the optimization with Reynolds-averaged Navier-Stokes (RANS) CFD solutions for the future improvement, the mesh topology has been extended to include anisotropic unstructured meshes which has been proven to be reliable in predicting the viscous wake[25]. In the next section, CFD solutions are based on the anisotropic meshes, different from the isotropic meshes used in this section, though the study is still focusing on the Euler-based optimization.

	Clean HWB				Integrated HWB				
Aerodynamic Characteristics	C_L	C_{D_ind} (10E-4)	C_{D_wave} (10E-4)	L/D	C_L	C_{D_ind} (10E-4)	C_{D_wave} (10E-4)	L/D	$C_{D\_wave\_cowl}$ (10E-4)
Baseline	0.1811	22.931	3.354	52.30	0.2023	39.99	2.969	38.22	1.177
Optimized	0.1811	19.546	0.491	67.67	0.2023	38.642	1.267	45.35	0.5369

Table 1: Comparisons of aerodynamic characteristics of the clean and integrated HWB.

B. Shape Design of the Nacelled HWB Configuration

The optimized design results of the integrated configuration is presented in Fig. 16 with baseline by its side. As discussed previously, the embedded nacelle significantly contributes to the lift increase at the region from root to 20%b_2, thus, the optimizer tends to mitigate loading at cowl region (90%c~TE, Fig.16-(a)). As a result, the shock strength is reduced as shown in Fig. 17. In addition to the change, the lift between 60%~90%c at the upstream of inlet became more negative to compensate the loading on the cowl for satisfying the trim condition. Thus, the root section came to have higher camber at 40~60%c region while those at 10~30%c and 60%c~TE became flattened for redistributing chord-wise load relative to the baseline. This shaping of upper surface around the inboard area helped to minimize drag with trim condition. Similar shape change occurred at 30%b_2 section as shown in Fig. 16-(b). On the other hand, the outboard loading change is straightforward since the effect of the nacelle is limited to the inboard up to 35%b_2, with less tip-twist angle (pitch up). The LE shock on the lower surface at 10%c (Fig.16-(c)), and TE shock (Fig.16-(d)) on the upper surface near 80%~90%c are removed. As a result, the chord-wise loading distribution becomes more stable, having peaks near the aerodynamic center. In Fig. 18, the baseline wing with a typical geometric washout gives an unbalanced spanwise lift distribution toward the center of the wing. This feature results in less wing efficiency, as most of the work is being done in the root sections. The current design gives a more balanced lift distribution and yields a smaller drag for the target lift. As a result, the wingtip twists down by 4.39 degree from the baseline, which means less wingtip unloading is needed to trim the integrated configuration. Figures 16-(a) and 16-(b) indicate the adjoint gradient search tends to prefer a slightly nose up design at the inboard area to enlarge the front loading to trim the aircraft. This explains why a higher lift than the elliptic distribution is observed. Though the optimized lift coefficient at root shows an improvement from its baseline, it may be still desirable to have the elliptic lift distribution at pitch trim.

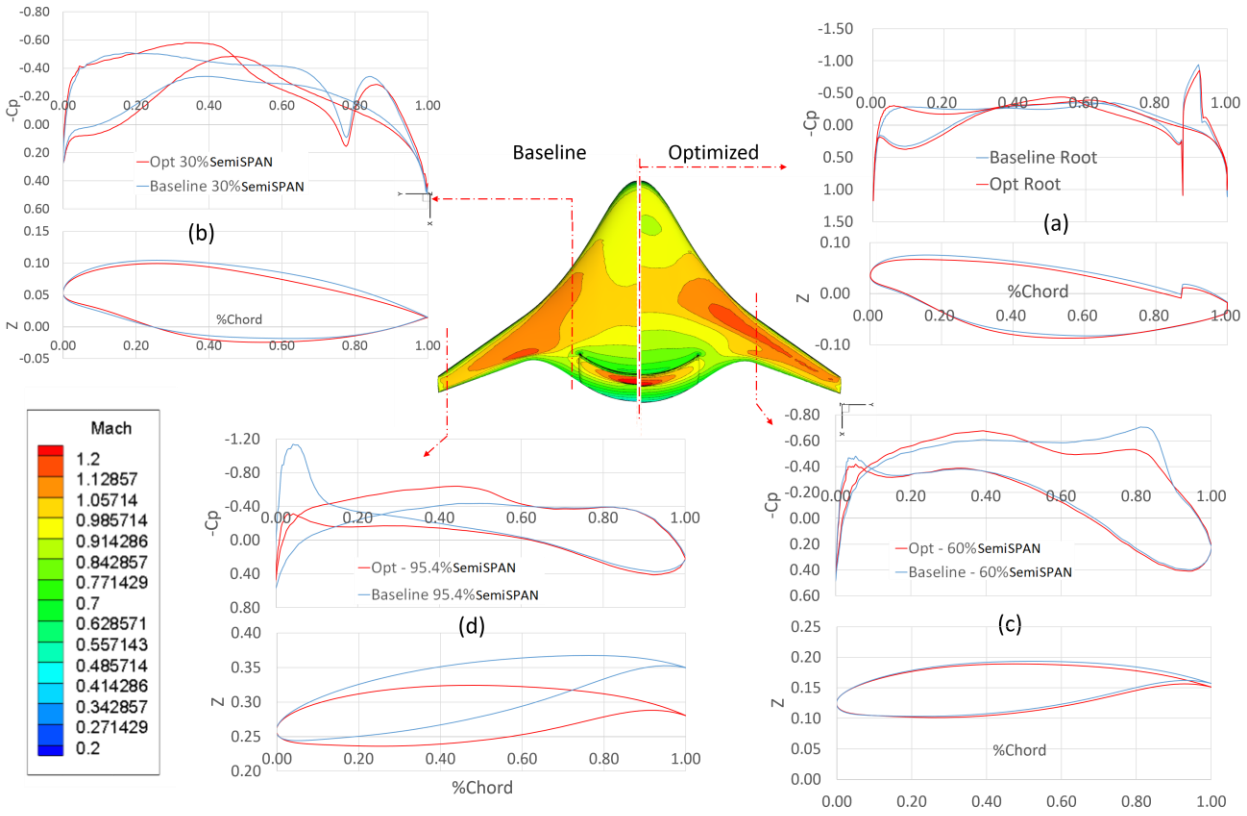

Figure 16. Optimized geometry comparison: baseline (left) vs optimized (right) of the integrated configuration. Here blue and red colors represent the baseline and the optimized design respectively in plots of the sectional pressure coefficient (C_p) distribution and sectional shape at sections (a)-(d).

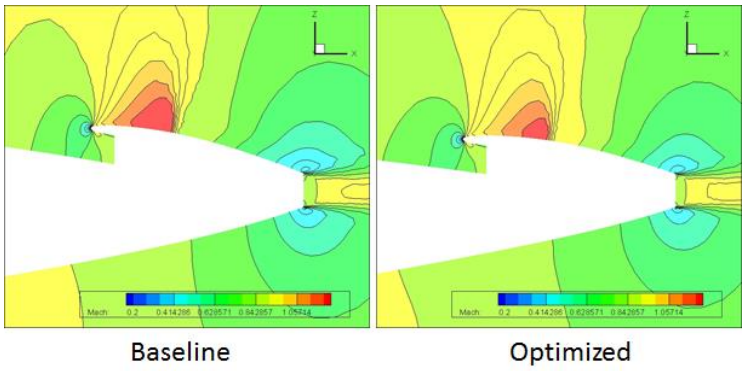

Figure 17. Mach contours around the nacelle/cowl of the integrated configuration at the symmetric plane.

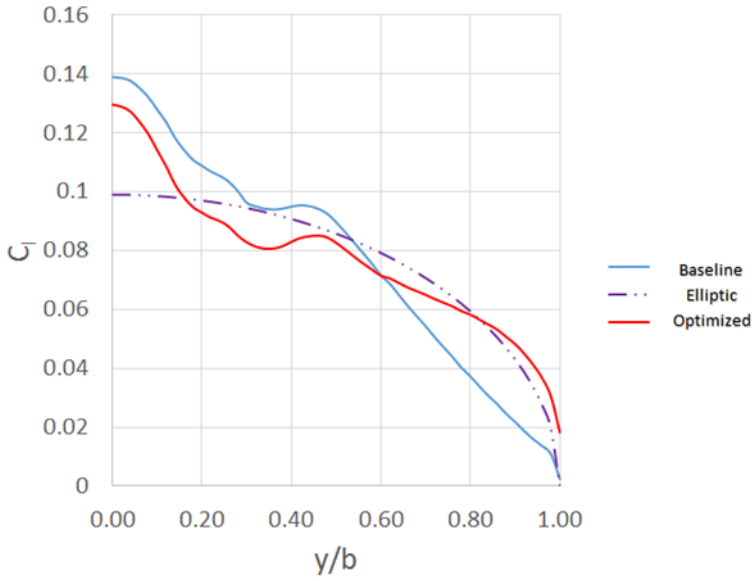

Figure 18. Spanwise loading comparison of the integrated configurations.

A nearly elliptic load was recommended in the Ref. 1 in which a reflexed center body blended with outboard supercritical airfoils. This challenge seems more difficult in the integrated configuration. One shortcoming in our approach is that the order of N used in the CST method is not high enough to yield adequate geometric degree of freedom near the trailing edge (90%c~TE), where nacelle is installed, as shown in Fig. 4. To approximate a reverse camber airfoil, a higher order, for instance $N = 14$, is planned for the future work. The other reason is that a local minimum could be trapped by the adjoint method. A global minimum may be obtained by using a non-gradient based optimization method, for instance, the genetic algorithms.

V. Conclusions

For an integrated HWB configuration, we have developed an approach that can easily include both the airframe and propulsion entities in the analysis and design process. We have described in detail in this paper the formulation that creates the HWB planform and 3-D wingbody and nacelle geometries that meet the mission and propulsion requirements for a 300-passenger transport by a concept configuration, N3X-DEP. An adjoint-based optimizer has been developed to improve aerodynamic performance. This computational tool is employed to minimize drag on the baseline configuration while satisfying the longitudinal static stability requirement. This task has been successfully accomplished by changing the HWB geometry and twisting. Reduction in induced and wave drags can be achieved,

resulting in a nearly 10 counts reduction in total drag under the trimmed condition. This study clearly demonstrates that the mutual interferences between the airframe and propulsion system is significant and its impact on the aerodynamic characteristics of the entire aircraft can be accounted for by a computational procedure as described above. It also affirms that it is possible to include detailed geometrical components at the early stage in the design cycle for a reliable quantitative aerodynamic evaluation. Future work will include viscous effects in the design analysis and a detailed representation of flows in the propulsion system.

References

[1] Liebeck, R. H., "Design of the Blended Wing Body Subsonic Transport," AIAA J. of Aircraft, Vol. 41, No. 1, 2004.
[2] Dowling, A. and Greitzer, E., "The Silent Aircraft Initiative- Overview," AIAA-2007-0452, Jan. 2007.
[3] Rosa Blanco, E., Hall, C. A. and Crichton, D., "Challenges in the Silent Aircraft Engine Design," AIAA-2007-0454, Jan. 2007.
[4] Thomas, R. H., Burley, C. L., and Olson, E. D., "Hybrid Wing Body Aircraft System Noise Assessment with Propulsion Airframe Aeroacoustic Experiments," AIAA 2010-3913.
[5] Smith, L. H., "Wake Ingestion Propulsion Benefit," J. Propulsion and Power, Vol. 9, 74-82, 1993.
[6] Nickol, C. L., "Silent Aircraft Initiative Concept Risk Assessment," NASA TM 2008-215112, 2008.
[7] Lyu, Z. and Martins, J., "Aerodynamic Design Optimization Studies of a Blended-Wing-Body aircraft," J. of Aircraft, Vol. 51, No. 5, 2014.
[8] Liou, M.-S. And Lee, B. J., "Minimizing Inlet Distortion for Hybrid Wing Body Aircraft," J. Turbomachinery, 134, May 2012.
[9] Felder, J., Kim, H. D., and Brown, G. V., "An Examination of the Effects of Boundary Layer Ingestion on Turboelectric Distributed Propulsion Systems," AIAA–2011–300, AIAA, 2011.
[10] Chima, R. V., "Rapid Calculations of Three-Dimensional Inlet/Fan Interaction," NASA Fundamental Aeronautics 2007 Annual Meeting, New Orleans, LA, Oct. 30–Nov. 1, 2007.
[11] Liou, M.-S., Kim, H. and Liou, M.-F., "Challenges and Progress in Aerodynamic Design of Hybrid Wingbody Aircraft with Embedded Engines," NASA/TM-2014-218309.
[12] Kim, H. and Liou, M.-S., "Flow Simulation of N3-X Hybrid Wing-Body Configuration," AIAA 2013-0221.
[13] Kim, H., Liou, M.-F. and Liou, M.-S. "Mail-Slot Nacelle Shape Design for N3-X Hybrid Wing Body Configuration," AIAA 2015-3805, AIAA Propulsion & Energy Forum 2015, Orlando, FL, 27-29 July 2015.
[14] Kulfan, B., "Universal Parametric Geometry Representation Method," Journal of Aircraft, Vol. 45, No. 1, 2008.
[15] Otani, I. and Maughmer, M. D., "The Conceptual Design of a Tailless Sailplane Having a Stabilizing Fuselage," Technical Soaring, Vol. 31, NO. 3, July 2007.
[16] Etkin, B., *Dynamics of Flight: Stability and Control*, 2nd Edition, John Wiley & Sons, New York, 1982.
[17] Laughlin, T. W., Corman, J. A., and Mavris, D. N., "A Parametric and Physics-Based Approach to Structural Weight Estimation of the Hybrid Wing Body Aircraft," AIAA 2013-1082, 51st AIAA Aerospace Sciences Meeting, Grapevine, TX, Jan. 2013.
[18] Kim, H., Harding D., Gronstal, D., Liou, M.-F. and Liou, M.-S.,"Design of the Hybrid Wing Body with Nacelle: N3-X Propulsion-Airframe Configuration" AIAA 2016-3875, 34th AIAA Applied Aerodynamics Conference, 13-17 June, 2016.
[19] Clancy, L.J.," Aerodynamics, Chapter 16, Pitman Publishing Limited, London, 1975.
[20] Kim, H.-J., Sasaki, D., Obayashi, S. and Nakahashi, K., "Aerodynamic Optimization of Supersonic transport Wing Using Unstructured Adjoint Method," AIAA J., Vol. 39, No. 6, June 2001.
[21] Vanderplaats, G., *Multidisciplinary Design Optimization*, First Edition, Vanderplaats Research & Development, 2007.
[22] Yamazaki, Q., Matsushima, K., Nakahashi, K., "Drag prediction, decomposition and visualization in unstructured mesh CFD solver of TAS code," Int. J. Numer. Meth. Fluids, 2008; 57; pp.417-436.
[23] Yamazaki, W., Matsushima, K. and Nakahashi, K., "Unstructured mesh drag prediction based on drag decomposition," ECCOMAS CFD, 2006.
[24] Reist, T. A. and Zingg, D. W., "Aerodynamic Shape Optimization of a Blended-Wing-Body Regional Transport for a Short Range Mission," AIAA 2013-2414, June, 2013.
[25] Kim, H., Liou, M.-F., and Liou, M.-S., "CFD Study of Propulsion-Airframe Interference on the N3-X Hybrid Wing-Body Configuration," ISABE-2015-20228, 22nd ISABE Conference, Oct. 2015.